sustainability

MDPI

Article

Developing General Equations for Urban Tree Biomass Estimation with High-Resolution Satellite Imagery

Jindong Wu

Department of Geography and the Environment, California State University Fullerton, Fullerton, CA 92831, USA; jindongwu@fullerton.edu; Tel.: +1-657-278-4020

Received: 25 July 2019; Accepted: 8 August 2019; Published: 12 August 2019

Abstract: Urban trees provide various important ecological services, the quantification of which is vital to sustainable urban development and requires accurate estimation of tree biomass. A limited number of allometric biomass equations, however, have been developed for urban species due to the prohibitive cost. Remote sensing has provided cost-effective means for estimating urban forest biomass, although the propagation of error in the estimation process is not well understood. This study aimed to offer a baseline assessment of the feasibility of estimating urban tree biomass with remote sensing-based general equations applicable to broad taxonomic groups by conducting a large urban tree inventory on a university campus. The biomasses of 191 trees of seven species from the inventory, separated into two categories (i.e., evergreen and deciduous), were calculated exclusively with urban-based species-specific allometric equations. WorldView-2 satellite imagery data were acquired to retrieve normalized difference vegetation index (NDVI) values at the location, crown, and stand levels. The results indicated that biomass correlated with NDVI in varying forms and degrees. The general equations at the crown level yielded the most accurate biomass estimates, while the location-level estimates were the least accurate. Crown-level spectral responses provided adequate information for delivering spatially explicit biomass estimation.

Keywords: urban trees; ecosystem services; dry weight; allometric equations; WordView-2; NDVI

1. Introduction

Urban landscapes are projected to continue to expand at unprecedented rates, increasing by 38.6 million hectares between 2010 and 2060 in the U.S. alone [1]. With 55% of the global population and over 80% of the U.S. population living in cities [2], urban-suburban land use and land cover play a progressively more important role in daily life issues, ecological processes, and climate change at both local and global scales [3]. As a basic element of urban-suburban environments, trees cover a significant area in cities. It was estimated that urban forests in the U.S. contain approximately 5.5 billion trees with an average urban tree canopy cover of 39.4% [1].

Rapid urbanization and population growth present a major cause of concern to the sustainability of cities [4]. Great efforts have been made to promote sustainable urban development [5,6]. The recently adopted United Nations' New Urban Agenda recognized the importance of urban greenspace in fostering social integration, economic growth, and environmental amelioration, and proposed a series of implementation plans for sustainably augmenting its social, economic, and environmental values [7]. Greenspace cover, including trees and grass, is considered one of the most significant sustainability indicator variables [8]. A number of large cities in the U.S., therefore, have initiated tree planting projects to restore their urban forests [9,10].

Numerous studies have demonstrated that urban trees contribute to the achievement of sustainable development goals by providing a variety of ecosystem services that are crucial to

human well-being [3,11–15]. In fact, urban trees supply all four types of ecosystem services identified by the Millennium Ecosystem Assessment, namely, provisioning, regulating, cultural, and supporting services [16]. As an example of provisioning services, wood biomass from urban forests is a potential source of timber and biofuels for wood products and energy generation [17]. Urban trees also provide regulating services by removing atmospheric carbon dioxide and storing carbon as biomass [18], moderating local and global temperatures [19,20], filtering airborne pollutants [21,22], reducing storm-water runoff, and recharging groundwater [20,23]. Perhaps the most common benefit to urban residents is the cultural role fulfilled by urban forests, which provide aesthetic and recreational enjoyment [24,25]. Each of these services is made possible because of the basic supporting services of urban trees, including the assimilation of mass and energy through photosynthesis and biogeochemical cycles, and the provisioning of habitats for diverse wildlife [26].

Some of the ecological benefits of urban trees are highly complementary and difficult to categorize as one of the four services. For instance, a recent broad epidemiological study reported that the risk of developing psychiatric disorders among people who only had access to sparse vegetation during childhood was up to 55% higher compared with those who were exposed to dense vegetation [27]. The exact causal health benefit of urban trees remains to be investigated, although it is probable that more than one type of ecosystem service may have played a beneficial role in reducing the risk of mental illness.

It is evident that the pursuit of sustainable urban development depends on an accurate understanding of urban ecosystem services, which requires baseline data on forest structure and functions [28]. Tree density and biomass either implicitly affect the ecosystem services described above, e.g., pollutant dispersion and deposition [21,22,29,30], transpirational cooling [19,29], and precipitation interception [20,23,31], or directly determines the quantity of the services such as carbon stored and sequestered and timber and biofuels garnered [17,18]. Biological quantities of vegetation (e.g., leaf areas and biomass), in addition to the area coverage and distribution, have been factored into sustainability indicators to evaluate the functions of urban vegetation in supporting the resilience of human-environment systems [32,33]. Reliable estimates of urban forest biomass are indispensable to monitor the progress towards attaining sustainability goals and develop management plans and practices for sustaining ecosystem services [34,35].

Field inventory-based biomass estimation, which is labor intensive and expensive, especially over a large area, typically requires destructive removal of tree components [36]. Thus, only a limited number of trees can be surveyed [36]. Repeated measurements over a period of years, which are essential for monitoring the change of urban forests, are particularly challenging to collect. To avoid prohibitively expensive and impractical sampling, allometric regression equations, which relate the volume or weight of a tree to readily observable attributes such as trunk diameter at breast height (DBH) or height, have been commonly used as an alternative non-destructive method [37]. Tree biomass can be either directly estimated or converted from the standing tree volume using wood density or specific gravity values for individual species.

A plethora of allometric biomass or volume equations have been generated for wildland trees [38–41]. However, very limited studies have developed allometric equations specifically for urban trees. In the published literature, only two studies have developed allometric volume equations for American street and park trees: One for 15 species in California [42] and the other for 11 species in Colorado [43].

Due to the scarcity of urban allometric equations, a number of studies have attempted to use allometric equations derived from measurements of identical or similar species in natural forests [18,44–47], or apply limited urban allometric equations across a range of urban settings or tree species based on taxonomic affiliations [43,48]. However, the edaphic and climatic conditions and management practices of open-grown trees in urban settings are dramatically different from those typical of trees in the wildland, altering the biomass partitioning of the urban trees [49]. The potential error of applying allometric equations developed for wildland trees directly to urban environments

could be substantial [50–52], ranging from −97% to 205% depending on the individual species and the sizes of the trees [43]. Biomass estimates could even vary from 27% less to 29% more when applying the allometric equation developed for an individual urban species in California to the same species in Colorado because of considerable differences in site conditions [43].

Considering the time and monetary cost of developing site- and species-specific allometric equations, it has been suggested to use general equations that are applicable to all species in a broad taxonomic grouping instead [43,53,54]. Such equations have been developed for 35 natural forest-grown genera on a national scale [39,40]. However, studies focused on developing allometric equations for general urban tree groups are scant [49], because urban-based equations over the entire range of site conditions are not available for compilation and synthesis [55].

Another approach to overcome the prohibitive cost associated with the development of allometric equations is to utilize remote sensing and geospatial techniques [49,56–60]. Remote sensing obtains information about the Earth's environment from a distance without the need for extensive field surveys over large areas. It has been used in several different ways as a non-destructive and cost-effective method for biomass estimation with varying degrees of success.

Generated with Light Detection and Ranging (LiDAR) technology, point cloud data have been regularly used to measure urban tree biomass directly [58,60–62] or extract basic silvicultural variables such as tree height and crown diameter, which are then applied to derive DBH for use in allometric equations [54,58,62–64]. The relationships of tree height and crown diameter to DBH, however, have not been well analyzed for urban species [49,63] and biomass estimation could easily be affected by data quality [56].

LiDAR data-derived structural characteristics have also been integrated with canopy photochemical properties retrieved from hyperspectral imagery to improve urban tree species identification [65], which would be helpful in selecting appropriate allometric equations for specific species [66]. However, the accuracy of species classification could change with the resolution of LiDAR and hyperspectral imagery, the fusion of structural and spectral features, and the utilization of different data processing algorithms [66–70].

Full coverage LiDAR and hyperspectral data of large areas are not always available and can be extremely expensive to acquire and process. High-resolution multispectral data, by contrast, are widely available, offering great opportunities to better resolve the spatial heterogeneous details of urban landscapes where land cover changes in a short distance [71–73].

Urban tree canopy maps derived from high-resolution multispectral imagery have been used to scale-up biomass estimates from limited field plots to the surrounding landscape [18,57]. However, tree misclassification, often caused by shadows [74], spectral confusion with other vegetation types [75], and insufficient field sampling, directly affects the accuracy of biomass estimation [76]. The reported accuracy of tree classification was 74.3% with QuickBird satellite imagery in Los Angeles, California [9] and 86.2% with digital color-infrared aerial imagery in Syracuse, New York [77].

The classification accuracy of high-resolution imagery was even lower at the species level [54]. An early study identifying seven urban tree species with IKONOS and WorldView-2 imagery only achieved an overall accuracy of 47.6%–57.0% and 53.7%–62.9%, respectively [78]. A more recent study showed that classification accuracy could improve by 10.7% on average if multitemporal imagery was used in the identification process [79].

For tree-level biomass estimation, individual tree crowns must be extracted from remote sensing imagery. However, automatic crown delineation is challenging because of the complexity of urban spaces [80]. Although sophisticated algorithms have been frequently used for crown segmentation [66,69,70,78,79], within-crown variations in brightness and difficulties in separating overlapping adjacent crowns could result in significant errors in both the number and sizes of crowns [60,81].

As the discussion above attests, the estimation of urban tree biomass is easily affected by errors in estimating spatial cover, species composition, and structural characteristics. However, it is not well

understood how these errors propagate and collectively affect biomass estimation [63,65]. Given these unknowns, this study was intended to demonstrate the realistic level of accuracy that can be achieved if the potential uncertainties in the methodological development and data processing were minimized.

Due to the high species diversity in urban forests, the current unlikelihood of distinguishing all species from multispectral imagery data, and relatively higher accuracy in classifying trees into general life forms [80,82], urban trees were divided into two broad types in this study, namely, evergreen and deciduous, which are usually sufficient for estimating ecosystem functions [78]. Considering the significant uncertainty associated with species assignation, tree biomass was calculated exclusively using urban-based species-specific formulas. Instead of using categorical land cover maps and scaling up plot-level measurements, continuous spectral features were directly incorporated into general equations to produce spatially explicit biomass estimates [59]. To avoid pitfalls associated with tree classification and crown segmentation, the tree stand cover was directly digitized from the high-resolution aerial images and the crown projected areas were generated with field-measured diameters.

Specifically, the objectives of this study were (1) to develop general equations for estimating the dry weight biomass of evergreen and deciduous urban trees with WorldView-2 satellite imagery at the location, crown, and stand levels, (2) to determine the level at which the biomass estimates would be the most accurate, and (3) to provide a baseline assessment of the feasibility of economically estimating urban tree biomass with remote sensing.

2. Materials and Methods

2.1. Study Area and Data Collection

The study area was the California State University Fullerton (CSUF) main campus, located in Southern California, approximately 40 km southeast of downtown Los Angeles (Figure 1). The mean annual temperature and precipitation of the area are 18.4 °C and 352.6 mm, respectively. Southern California has a typical Mediterranean climate characterized by mild and wet winters and hot and dry summers.

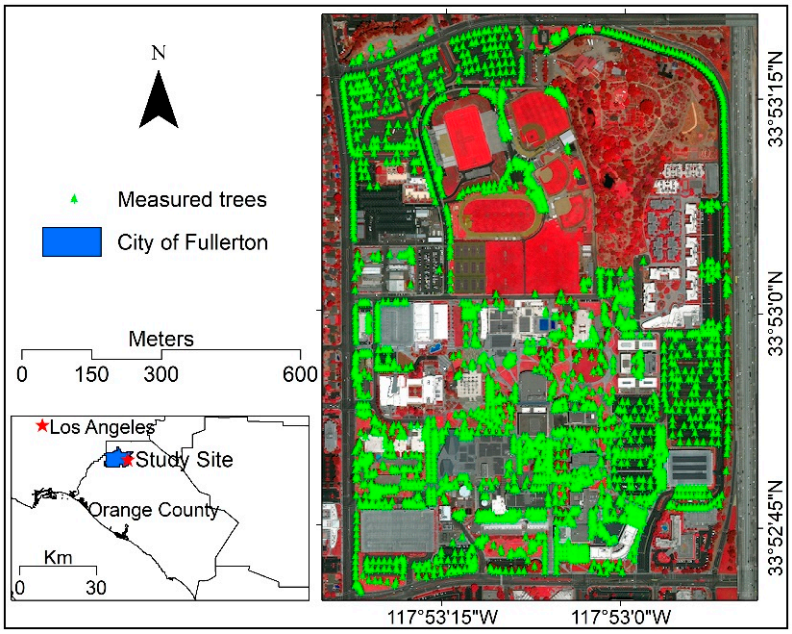

Figure 1. The geographical location of the study site where 2185 trees were measured on the California State University Fullerton main campus and the WorldView-2 satellite imagery (acquired on 16 June 2012) was used to derive normalized difference vegetation index.

Land use and land cover of the rectangular 95.5 ha campus is dominated by high-density institutional land development such as classroom buildings, parking lots, walking paths, trees, and turf grass. The Fullerton Arboretum and Botanic Garden of the University, located at the northeast end of the campus, was masked in the study because trees in the Arboretum are unique and not typical of those in Southern California urban-suburban environment.

2.1.1. Remote Sensing Imagery Data

WorldView-2 multispectral satellite imagery of the study area was acquired on 16 June 2012 under clear sky conditions. The imagery was the best available high-resolution satellite data coincident with the ground measurement described below. With 11-bit radiometric resolution, the WorldView-2 sensor has 5 visible bands (0.4–0.45 μm, 0.45–0.51 μm, 0.51–0.58 μm, 0.585–0.625 μm, and 0.63–0.69 μm), 1 red edge band (0.705–0.745 μm), and 2 near infrared (NIR) bands (0.77–0.895 μm and 0.86–1.04 μm). The imagery, with a spatial resolution of 2 m, was taken at a sun elevation angle of 75.0°, an off-nadir view angle of 5.5°, and a maximum target azimuth of 297.0°. The images were geometrically rectified with a root mean square error (RMSE) of 0.61 m and radiometrically and atmospherically corrected [83,84]. An Orange County color aerial orthophotograph (spatial resolution, 0.15 m), collected on 19 April 2011, was used as ancillary data to aid in tree stand delineation as described below.

2.1.2. Field Tree Measurement and Tree Species Selection

A large field inventory was conducted in 2012 to collect tree location and attribute data on the CSUF main campus. Most measurements were completed between June and October while supplementary measurements lasted until March 2013. In total, 2185 trees were individually visited for tagging, identification, and measurement. All data were recorded with ArcPad 10 mobile geographic information system (GIS) and transferred wirelessly to an enterprise GIS geodatabase through the campus's internet network [85].

Tree locations were measured with a Trimble GeoExplorer 2008 series (GeoXT) global positioning system (GPS) unit that was capable of providing sub-meter positional accuracy under optimal conditions. However, in areas surrounded by tall buildings that hindered the acquisition of strong GPS signals, it was difficult to obtain accurate GPS readings. For trees in these areas, spatial locations were manually plotted using elements of the campus as points of reference. Further verification showed that the overall positional accuracy of these data points was actually higher than the GPS readings.

The measured biophysical tree attributes included the number of trunks, average trunk diameter at breast height (1.37 m above ground, DBH), tree height, crown height, and crown width. DBH was measured with a diameter tape. For trees with multiple trunks, the average DBH values were recorded as well as the total number of trunks at breast height. Tree height, crown width, and crown height were measured with a TruPulse 360B laser range finder, which had a distance accuracy of ± 0.3 m and inclination accuracy of ± 0.25°. The crown diameter was determined by averaging crown width along the long and short axes.

The family, genus, and species were identified for each measured tree in addition to its common and scientific names. In all, 111 unique species were identified over the course of the tree inventory. Metal identification tags engraved with permanent numerical numbers were nailed into the trunks of individual trees at approximately the same location that DBH was measured. Tree conditions, planting dates, trimming schedule, and fertilization schedule were also documented for landscaping operations.

Among all species identified in the tree inventory, 7 were selected in this study based on the availability of species-specific urban allometric equations [42]. The 7 species were grouped into 2 categories: Evergreen trees (*Cinnamomum camphora* and *Magnolia grandiflora*) and deciduous trees (*Jacaranda mimosifolia*, *Liquidambar styraciflua*, *Platanus* × *acerifolia*, *Ulmus parvifolia*, and *Pistacia chinensis*) (Table 1). Altogether, 191 trees (27 evergreen trees and 164 deciduous trees) in the 7 species were selected from the inventory. For each category, the trees were split into 2 independent datasets by

random selection of the total samples: 80% of the trees were used in the development of general biomass equations and 20% of the trees were used in the cross-validation of the equations.

Table 1. Seven selected tree species and their common names, sample sizes (*n*), ranges of diameter at breast height (DBH) and height specified in the urban-based allometric equations [42], and measured DBH and height means.

Tree Type	Species	Common Name	*n*	DBH (cm)		Height (m)	
				Range	Mean	Range	Mean
Evergreen	*Cinnamomum camphora*	Camphor Tree	8	13.2–68.8	23.2	5.2–17.1	7.8
	Magnolia grandiflora	Southern Magnolia	19	14.5–74.2	33.3	5.8–18.9	9.8
Deciduous	*Jacaranda mimosifolia*	Jacaranda	58	17.3–59.7	38.6	6.9–17.5	11.6
	Liquidambar styraciflua	American Sweet Gum	27	14.0–54.4	30.2	7.3–20.0	11.6
	Platanus × *acerifolia*	London Planetree	47	15.5–73.9	24.2	7.9–27.9	10.4
	Ulmus parvifolia	Chinese Elm	9	17.3–55.9	42.4	7.6–18.9	15.2
	Pistacia chinensis	Chinese Pistache	23	12.7–51.3	16.7	6.7–15.8	7.2

2.2. Tree Crown Projected Area Generation and Stand Cover Delineation

The commonly used circular shape was assumed in the delineation of the tree crowns [86]. Centered on individual tree locations and using field-measured crown diameter, circular crown projected areas were generated with the Geospatial Modelling Environment (GME) 0.7.4.0 [87] (Figure 2). Tree stand cover was digitized over the Orange County color aerial orthophotograph in ArcGIS 10.3. [88]. Contiguous patches of trees that were spatially distinguishable from adjacent communities were traced from the aerial photography directly on the computer screen, regardless of age class distribution, species composition, and population structure. Tree sites were physically inspected whenever aerial photography did not provide sufficient representation. In total, 135 tree stands were found to only contain selected species in this study. It is noteworthy that the delineated tree stands or patches were considered homogeneous units in this study; they might be different from conventional tree stands defined in forestry [65]. Tree stands were also divided into 2 independent datasets by random selection of the total samples: 80% of the stands were used in developing general equations at the stand level and 20% of the stands were used in cross-validating the equations.

2.3. Dry Weight Biomass Estimation

The dry weight biomass (DWB) of individual trees was calculated based on the estimation of tree volume with the allometric equations [49].

$$DWB_i = d{\cdot}t{\cdot}\rho_i{\cdot}V_i, \quad (1)$$

where DWB_i (kg) is the total dry weight biomass of species i with volume V_i (m^3); ρ_i ($kg{\cdot}m^{-3}$) is the species-specific wood density [89,90]; t (1.28) is the total biomass conversion factor to include belowground biomass based on the average root-to-shoot ratio [91,92]; d (0.48 for evergreen and 0.56 for deciduous) is the constant to convert fresh weight to dry weight [45].

Both sets of the allometric equations that have been developed for urban trees in California were applied in this study: Local volume equations based solely on DBH and standard volume equations based on both DBH and tree height [42] (Table 2). These allometric equations were developed for trees with certain sizes in terms of DBH and height. They are not applicable to trees of other sizes. The extrapolation of allometric equations beyond the original ranges of DBH or height can lead to seriously biased estimates [55]. Therefore, trees were excluded from the computation if their sizes fell outside the ranges of DBH or height specified in the allometric equations (Table 1).

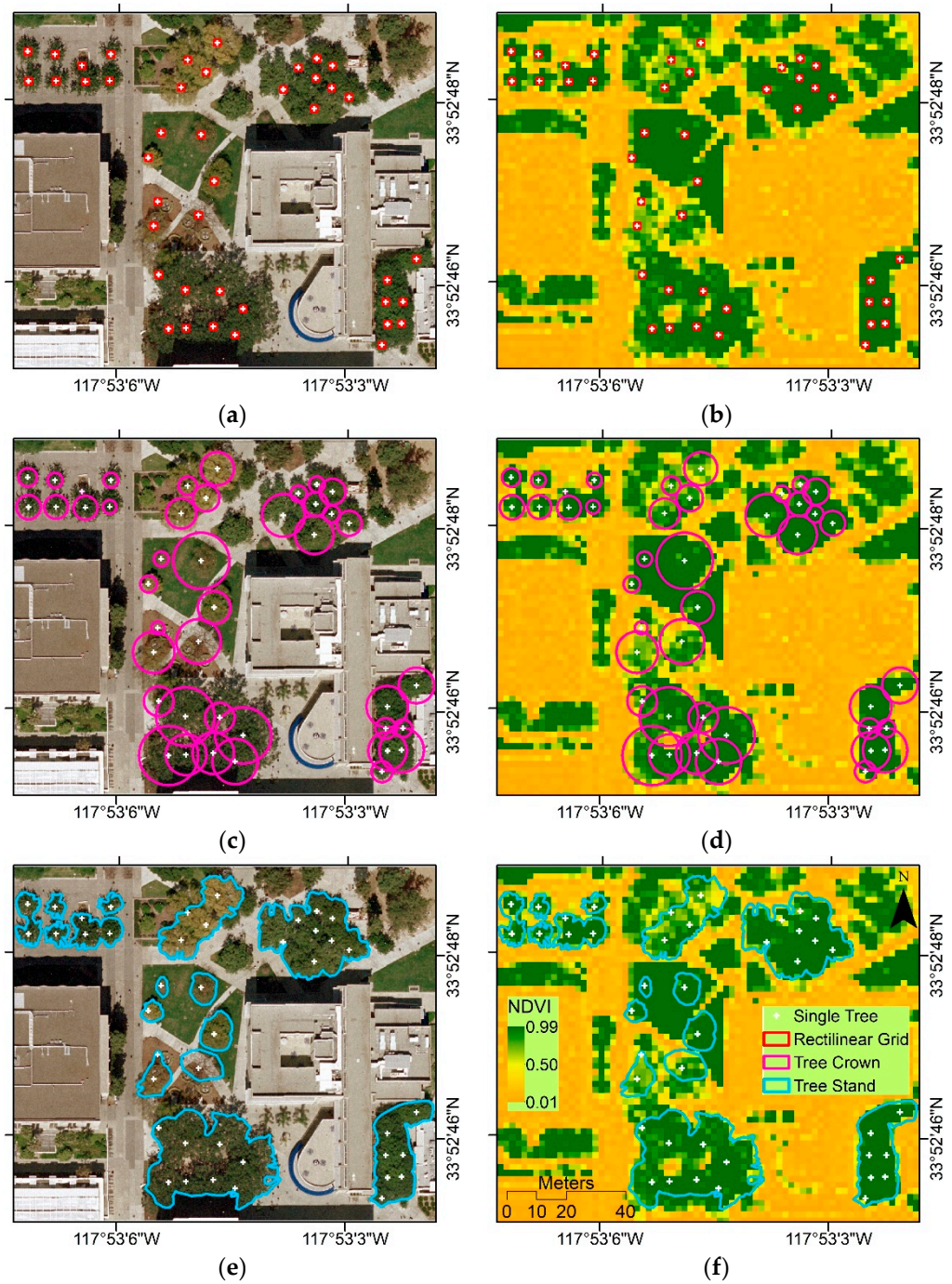

Figure 2. Illustration of three approaches for biomass estimation based on tree locations (**a**), crowns (**c**), and stands (**e**) on a portion of the California State University Fullerton main campus. Normalized difference vegetation index (NDVI) values, derived from the WorldView-2 satellite imagery (acquired on 16 June 2012), were computed for individual tree locations with bilinear interpolation (**b**). NDVI pixel values were aggregated for crown (**d**) and stand (**f**) level estimations.

Table 2. Local and standard allometric volume equations adapted from the study in California for the seven selected tree species [42] [i].

Species	Local Volume Equation	Standard Volume Equation
Cinnamomum camphora	$V_i = 0.083856DBH^{2.534660}$	$V_i = 0.080707DBH^{2.134803}H^{0.634042}$
Magnolia grandiflora	$V_i = 0.055903DBH^{2.622015}$	$V_i = 0.050347DBH^{2.070408}H^{0.845627}$
Jacaranda mimosifolia	$V_i = 0.100832DBH^{2.486248}$	$V_i = 0.080063DBH^{2.185780}H^{0.548045}$
Liquidambar styraciflua	$V_i = 0.079872DBH^{2.560469}$	$V_i = 0.063076DBH^{2.315815}H^{0.415711}$
Platanus × *acerifolia*	$V_i = 0.058962DBH^{2.673578}$	$V_i = 0.048510DBH^{2.436420}H^{0.391682}$
Ulmus parvifolia	$V_i = 0.069001DBH^{2.639347}$	$V_i = 0.060906DBH^{2.324812}H^{0.493171}$
Pistacia chinensis	$V_i = 0.039250DBH^{2.808625}$	$V_i = 0.032899DBH^{2.191572}H^{0.943669}$

[i] V_i (10^{-3} m^3), DBH (cm), and H (m) represent tree volume, diameter at breast height, and height, respectively.

Given that DWB estimates calculated with two sets of equations were found to be highly correlated (The Spearman's correlation coefficient (0.99) is significant at $\alpha = 0.01$), as has been reported by other studies [41], only the estimation with DBH was used hereafter in all analysis. Stand biomass was estimated by aggregating the DWB of individual trees that were located within each stand. Tree stands that comprised species other than the 7 selected species were excluded from the calculation due to the unavailability of allometric equations.

2.4. Vegetation Index Derivation

Normalized difference vegetation index (NDVI) imagery was generated with the radiometrically corrected visible band 5 and NIR band 7 of the WorldView-2 imagery [93]. NDVI values were retrieved separately for individual tree locations, crowns, and stands (Figure 2). At the location level, NDVI values (i.e., $NDVI_b$) were derived with bilinear interpolation of 4 nearest pixels, assuming that the peak of canopy reflectance was located at the treetop points [94]. Crown-level NDVI (i.e., $NDVI_c$) and stand-level NDVI (i.e., $NDVI_s$) were calculated as the arithmetic sum of all pixels within the crown projected area and tree stand, respectively.

$$NDVI_c = \sum_{i=1}^{m} NDVI_i, \quad (2)$$

$$NDVI_s = \sum_{i=1}^{n} NDVI_i, \quad (3)$$

where $NDVI_i$ is the NDVI value of pixel i situated within the crown projected area or stand. m and n are the total number of pixels within the crown projected area and stand, respectively. Tree crowns were processed sequentially to avoid potential underestimation of $NDVI_c$ caused by the overlap of crown polygons, which is commonly found in urban forests [87].

2.5. Regression Analysis and Statistical Evaluation

Multiple regressions were conducted to reveal the best relationships between DWB and NDVI at the location, crown, and stand levels. A logarithmic transformation was applied to DWB because variance tends to increase with the size of trees [92,95,96]. The ordinary least squares regression was performed between the transformed DWB and NDVI derived for tree locations (i.e., $NDVI_b$). Separate loglinear regressions were analyzed for evergreen and deciduous trees.

$$\ln(EDW_t) = b_1 NDVI_b + a_1, \quad (4)$$

$$\ln(DDW_t) = b_2 NDVI_b + a_2, \quad (5)$$

where EDW_t and DDW_t are the DWB of a single evergreen and deciduous tree, respectively. (b_1, a_1) and (b_2, a_2) are the 2 sets of corresponding regression coefficients. At the crown and stand levels, NDVI

values were also logarithmically transformed to makes it possible to apply linear regression. Log-log linear regression were performed between DWB and crown-level NDVI (i.e., $NDVI_c$).

$$\ln(EDW_t) = b_3 \ln(NDVI_c) + a_3, \quad (6)$$

$$\ln(DDW_t) = b_4 \ln(NDVI_c) + a_4, \quad (7)$$

where (b_3, a_3) and (b_4, a_4) are the regression coefficients for evergreen and deciduous trees, respectively. Log-log linear regression was also carried out between stand DWB and stand-level NDVI (i.e., $NDVI_s$).

$$\ln(DW_s) = b_5 \ln(NDVI_s) + a_5, \quad (8)$$

where DW_s is the total DWB of an entire tree stand as defined before. b_5 and a_5 are the regression coefficients. Evergreen and deciduous trees were not separated since both could reside in the same tree stand.

All regressions were run with IBM SPSS Statistics (version 25) [97]. The significance of the regressions was evaluated with the *t*-test. To assess the accuracy of these regression models for estimating DWB in measured units, Equations (4) and (5) were converted to the following exponential forms for individual evergreen and deciduous trees at the location level:

$$EDW_t = \alpha_1 e^{\beta_1 NDVI_b}, \quad (9)$$

$$DDW_t = \alpha_2 e^{\beta_2 NDVI_b}, \quad (10)$$

Equations (6)–(8) were converted to the following power functions to estimate DWB at the crown and stand levels.

$$EDW_t = \alpha_3 (NDVI_c)^{\beta_3}, \quad (11)$$

$$DDW_t = \alpha_4 (NDVI_c)^{\beta_4}, \quad (12)$$

$$DW_s = \alpha_5 (NDVI_s)^{\beta_5}, \quad (13)$$

where α_i and β_i (i = 1, 2 … 5) are the transformed coefficients from the corresponding regression equations.

Four different criteria were computed to cross-validate the performance of Equations (9)–(13) [95,98]: The linear regression through the origin, the paired sample *t*-test, the root mean square error (RMSE), and the mean relative difference (MRD). The independent data points reserved for validation were first tested for normality with the Shapiro-Wilk test [97]. Estimates of DWB with NDVI were plotted against the corresponding estimates with the allometric equations. The slope of the linear regression between the 2 estimations through the origin directly indicated any differences under normal distributions. The paired sample *t*-test was used to evaluate if these differences were statistically significant. RMSE is the standard deviation of absolute differences while MRD is the average of relative differences between two estimations.

3. Results

3.1. DWB–NDVI Relationships

The regression analysis showed that two different types of relationships existed between DWB and NDVI (Figure 3). The logarithmically transformed DWB appeared to change linearly with NDVI at the location level for both evergreen and deciduous trees. However, at the crown and stand levels, logarithmic relationships were found significant between transformed DWB and NDVI. Consequently, DWB could be described as an exponential function of NDVI at the location level and as a power function of NDVI at the crown and stand levels.

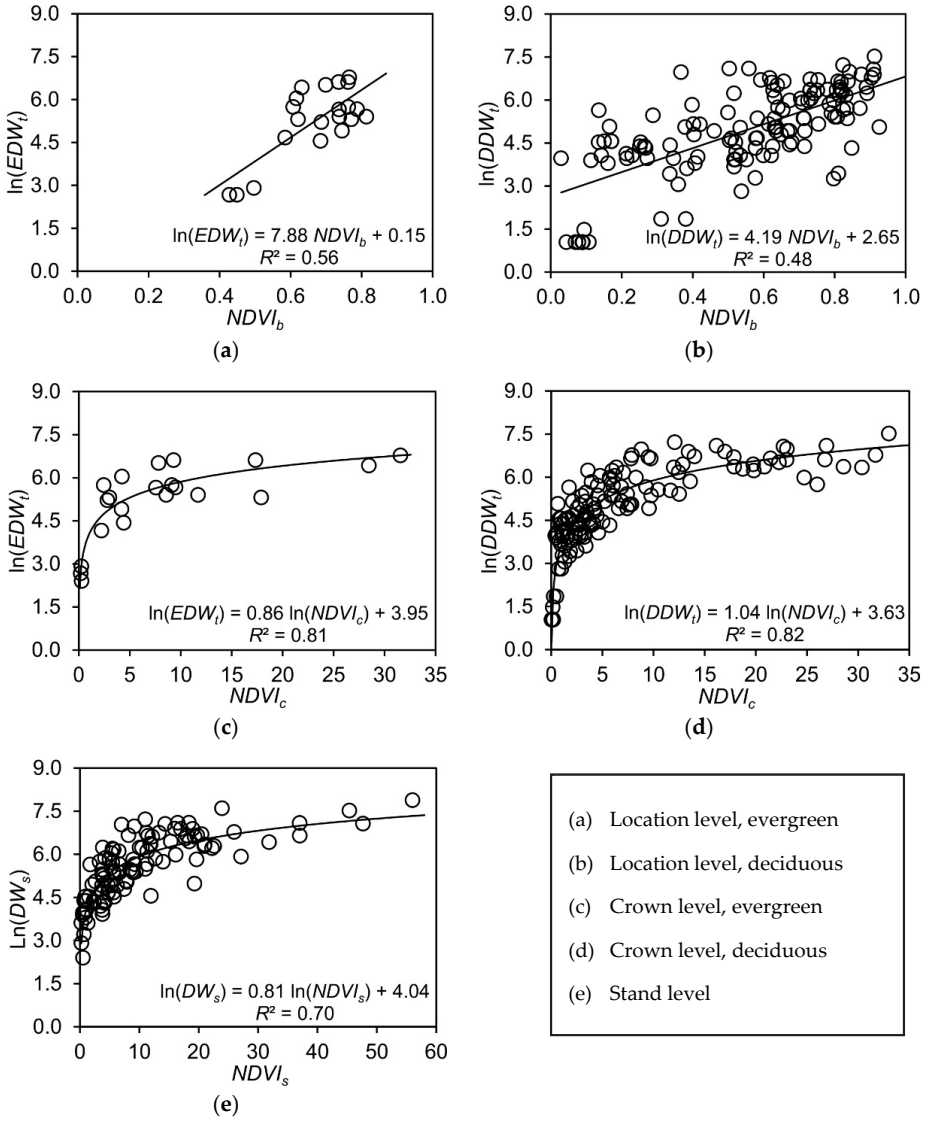

Figure 3. Regressions between tree dry weight biomass and normalized difference vegetation index derived from the WorldView-2 imagery (acquired on 16 June 2012), at the location ($NDVI_b$), crown ($NDVI_c$), and stand levels ($NDVI_s$). EDW_t and DDW_t are the dry weight biomass of a single evergreen ((**a**) and (**c**)) and deciduous tree ((**b**) and (**d**)), respectively. DW_s is the dry weight biomass of an entire stand (**e**).

In the established DWB–NDVI relationships, DWB showed varying degrees of correlation with NDVI (Table 3). While the log-log linear correlations for evergreen and deciduous trees were significant at the crown level ($R^2 = 0.81$ and 0.82, respectively), R^2 values of the loglinear correlations were low (~0.5) for both types of trees at the location level. At the stand level, transformed DWB was moderately but significantly correlated with transformed NDVI with a R^2 of 0.7. Overall, the variations in DWB explained by the regression models were greater at the crown and stand levels than those at the location level.

The strength of the correlations was comparable between evergreen and deciduous trees, although the parameters in the DWB–NDVI relationships varied considerably. As indicated by the low standard errors, the estimates of regression coefficients attained higher precision for the crown- and stand-level DWB–NDVI relationships than that for the location-level relationships. In fact, the constant coefficient of the loglinear regression for evergreen trees at the location level was not statistically significant.

Table 3. Statistical models for estimating tree dry weight biomass with location-, crown-, and stand-based normalized difference vegetation index (NDVI) derived from the WorldView-2 imagery [ɨ].

	Location Level				Crown Level				Stand Level	
	Evergreen	*t**	Deciduous	*t**	Evergreen	*t**	Deciduous	*t**		*t**
n	21		131		21		131		108	
b_{1-5}	7.88 (1.38)	4.95	4.19 (0.38)	10.97	0.86 (0.09)	9.15	1.04 (0.04)	23.64	0.81 (0.05)	15.88
a_{1-5}	0.15 (0.93)	0.16	2.65 (0.23)	11.47	3.95 (0.19)	21.35	3.63 (0.08)	45.95	4.04 (0.11)	35.44
R^2	0.56		0.48		0.81		0.82		0.70	
SE	0.83		1.09		0.58		0.66		0.61	

[ɨ] n is the sample size. b_{1-5} and a_{1-5} are, respectively, the slope and constant coefficients of the regression between logarithmically transformed dry weight biomass and NDVI (Equations (4) and (5)) or logarithmically transformed NDVI (Equations (6)–(8)). Values in parentheses are the standard errors of corresponding parameters and SE is the standard error of the regression. R^2 is the coefficient of determination. *t** indicates that the statistical test of the regression is significant at $\alpha = 0.05$ except for a = 0.15.

3.2. Comparison of DWB Estimations

Table 4 shows the parameters that were used to estimate DWB with Equations (9)–(13) at the location, crown, and stand levels. The results indicated that there was general agreement between biomass estimated with NDVI and that with the allometric equations (Figure 4). The R^2 ranged from 0.47 for evergreen and 0.63 for deciduous trees at the location level, 0.81 at the stand level, to 0.83–0.84 at the crown level (Table 5). However, the comparison showed that DWB estimates based on NDVI were consistently lower than those based on the allometric equations.

The slope of the regression between NDVI-based and allometric equation-based estimations was only 0.55 and 0.51 for evergreen and deciduous trees, respectively, at the location level, increasing slightly to a higher value of 0.62 at the stand level. The regression slope reached its highest value, though it was still less than 1.0, at the crown level (0.77 and 0.86 for evergreen and deciduous trees, respectively). The underestimation was also shown by the negative MRD values for all three NDVI-based methods, varying from −23.25% for evergreen and −12.60% for deciduous trees at the crown level, −13.16% at the stand level, to as high as −39.57% and −29.58% at the location level for evergreen and deciduous trees, respectively.

It appeared that the crown-level NDVI was able to estimate DWB at the highest accuracy with the largest regression slope and lowest MRD while the location-level NDVI was the worst. This was also confirmed by the paired sample *t*-test and RMSE in addition to the slope and MRD. The paired sample *t*-test showed that DWB estimates based on NDVI and those based on the allometric equations were not statistically different for both types of trees at the crown level. However, the two estimations were significantly different from each other at the point and stand levels.

Table 4. Transformed statistical models for estimating tree dry weight biomass with location-, crown-, and stand-based normalized difference vegetation index (NDVI) [ɨ].

	Location Level		Crown Level		Stand Level
	Evergreen	Deciduous	Evergreen	Deciduous	
α_i	1.16	14.15	51.94	37.71	56.83
β_i	7.88	4.19	0.86	1.04	0.81

[ɨ] α_i and β_i are the transformed coefficients of the corresponding regression relationships (Equations (9)–(13)) between dry weight biomass and NDVI.

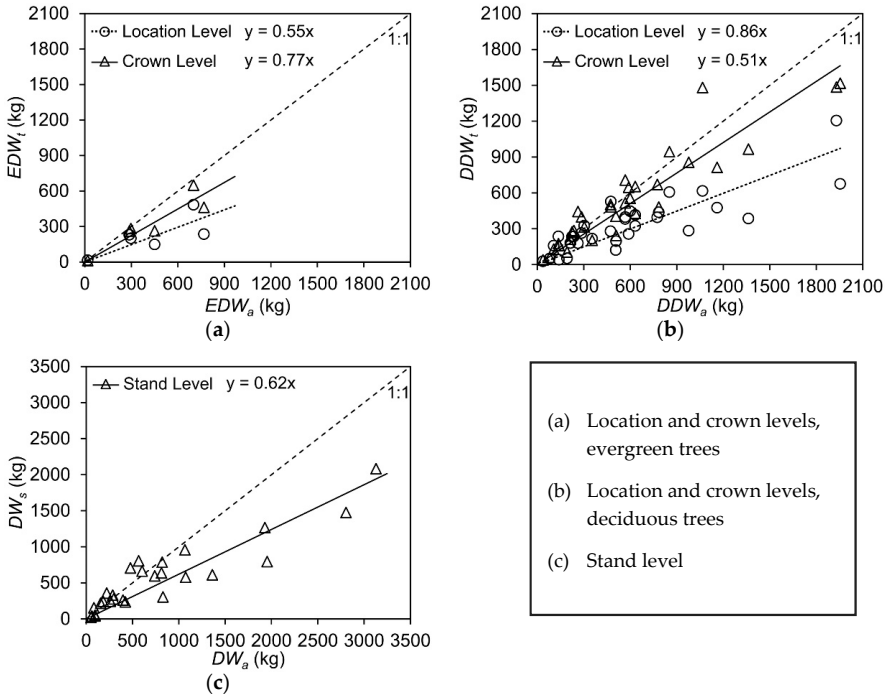

Figure 4. Comparison of tree dry weight biomass computed with the species-specific allometric equations (i.e., EDW_a, DDW_a, and DW_a) and estimated with the normalized difference vegetation index (NDVI) based general equations (i.e., EDW_t, DDW_t, and DW_s) at the location, crown, and stand levels, respectively. EDW_a and EDW_t are the dry weight biomass of a single evergreen tree (**a**). DDW_a and DDW_t are the dry weight biomass of a single deciduous tree (**b**). DW_a and DW_s are the dry weight biomass of an entire stand (**c**).

Table 5. Statistical evaluation of tree dry weight biomass estimation with location-, crown-, and stand-based normalized difference vegetation index (NDVI) derived from the WorldView-2 imagery [ɨ].

	Tree Type	*n*	*W*	t_p	*b*	R^2	*t**	RMSE (kg)	MRD (%)
Location Level	Evergreen	6	0.98 [+]	3.19 [+]	0.55	0.47	4.35	269.18	−39.57
	Deciduous	33	0.91 [+]	4.20 [+]	0.51	0.63	12.69	403.79	−29.58
Crown Level	Evergreen	6	0.84 [+]	1.74	0.77	0.83	10.39	148.51	−23.25
	Deciduous	33	0.95 [+]	1.25	0.86	0.84	20.91	193.48	−12.60
Stand Level		27	0.89 [+]	2.75 [+]	0.62	0.81	16.97	471.51	−13.16

[ɨ] *n* is the sample size. *W* is the statistic of the Shapiro-Wilk test for normality. t_p is the statistic of the paired sample *t*-test for tree dry weight biomass differences between estimations with NDVI and with the allometric equations. *b* is the slope of regression between two estimations. *t** indicates that the statistical test of the regression is significant at $\alpha = 0.05$. R^2 is the coefficient of determination. RMSE is the root mean square error and MRD is the mean relative difference. [+] indicates a normal distribution of paired data points or a significant difference within the pair at $\alpha = 0.05$.

The RMSE of the crown-level estimates was 148.51 kg and 193.48 kg for evergreen and deciduous trees, respectively, while the corresponding location-level RMSE was as large as 269.18 kg and 403.79 kg, approximately twice as much as those at the crown level. Although the RMSE of the stand-level estimates (i.e., 471.51 kg) was significantly larger than that at the location and crown levels. It should be noted that the RMSE of a stand, which may include multiple trees, was incomparable to the RMSE of individual trees at the location and crown levels.

4. Discussion

Even though the field measurements were taken for a variety of species with different tree conditions, the DWB–NDVI correlations were found to be significant, mainly at the crown and stand levels, suggesting that the spectral features of urban trees can provide useful information for biomass estimation. Previous studies have reported that Landsat imagery-derived NDVI showed positive non-linear correlation with aboveground urban tree biomass at the field-plot scale [59,99]. The relationship between DWB and NDVI appeared to be logarithmic and exponential in the Boston and Syracuse metropolitan areas in the respective studies.

This study confirmed that the nonlinear relationship also existed at the individual tree and stand levels when using high-resolution remote sensing imagery. However, DWB was found to change significantly with NDVI as a power function, instead of a logarithmic or exponential function. The challenges of using low-resolution Landsat data in differentiating grass, shrubs, and trees, which could differ substantially in their contributions to the biomass estimation of a field plot, likely attributed to the variation of DWB–NDVI relationships. Coincidentally, the power functional relationships of DWB–NDVI developed in this study have the same mathematical form as the allometric DWB–DBH equations developed from field inventories.

All DWB–NDVI relationships underestimated tree biomass. The underestimation is consistent with the previous studies of biomass equations that generalized 26 urban-based species-specific allometric equations [49]. Part of the underestimation was probably caused by the inherent bias in applying logarithmic transformations when developing these equations [95,96,98,100]. It was found that logarithmic transformations could cause a slight downward bias when equations are converted back to compute biomass in measured units. Studies attempting to remedy the problem did not result in more accurate estimates, particularly for small sample sizes [40,101]. Furthermore, the potential underestimation could not be accounted for even if the weighted nonlinear regression was used without logarithmic transformations [43].

Although reasonably accurate biomass estimation was achieved, particularly at the crown level, with approximately 80% of variance in the transformed DWB explained by the regression, the relatively large RMSE and MRD values indicated that high variability existed in DWB estimates due to the variations in individual tree conditions. Inaccuracies in measurement and data may also have contributed to the high variability of biomass estimates. For instance, accurate measurement of crown diameter was difficult to achieve in the field, especially for those trees with irregular shapes. The shape of crowns was assumed to resemble a circle, although studies have found that crown shapes are often more eccentric [102] and that the circular crown projection could underestimate crown projected area up to 16% [103].

In addition, the total DWB estimates were based on the average root-to-shoot ratio, which was generalized from a global forest data synthesis [91]. It has been largely agreed that biomass allocation to roots is subject to various biotic and abiotic factors, although the relationship between these factors and root-to-shoot ratio are not clear. According to the very limited studies of urban trees, root-to-shoot ratios change significantly across species and over time [104]. Likewise, wood density values used in DWB estimation were not specific to urban species because no urban-based studies were found in the literature. However, studies have observed noticeable changes in wood density if trees are subjected to different nutrient and water conditions [105].

Like all statistical relationships, remote sensing-based biomass equations developed in this study are only recommended to be applied to the trees that are under similar urban growth conditions. Although 2185 trees of 111 species were measured in the field inventory, only 191 trees of 7 species matched with the urban-based allometric equations that are currently available. In particular, there were only 27 trees of 2 evergreen species. More field measurements of street and park trees are necessary to further assess the equations developed in this study. The lack of ground-based biometric data of urban trees either calculated with species-specific allometric relationships or measured in the

field remains a serious limitation to the development and validation of remote sensing-based methods for biomass estimation.

Biomass calculated with the remote sensing-based regression models was specific to individual trees and stands, thus eliminating the need of field plots and having minimal scaling effects compared to the conventional approaches that rely on categorical land use and land cover maps. The stand-level estimates were reasonable but lower than the crown-level estimates. The low estimation could likely be explained by the unaccounted clumping effect on the stand-level NDVI, particularly in large tree stands where canopy leaves from multiple trees are heavily clustered.

From the remote sensing perspective, the best results produced by the crown-based method indicated that accurate crown delineation would be essential to the estimation of urban tree biomass. The increasing availability of high-resolution imagery, such as the recent acquirement of 0.6 m color infrared aerial imagery in the National Agriculture Imagery Program, provides new opportunities in isolating and measuring individual tree crowns, even irregular ones for large area applications. More research is needed to resolve the technical difficulties in separating overlapping adjacent crowns, possibly with the proper integration of high spatial resolution spectral responses with structural features derived from LiDAR data.

5. Conclusions

In spite of the fact that it is imperative to the quantification of urban forest ecosystem services and the development of management plans and practices for sustainable cities, urban tree biomass is difficult to estimate owing to the expensive cost of destructive removal of tree components, limited species-specific and site-specific allometric equations, and uncertainties associated with remote sensing data processing and methodological development. This study assessed the feasibility and baseline accuracy of economically estimating urban tree biomass with high-resolution multispectral satellite imagery when the various potential uncertainties were minimized. The results showed that biomass correlated in varying forms and degrees with NDVI derived from the WorldView-2 satellite imagery at the location, crown, and stand levels. While relatively high variability existed, the general DWB–NDVI nonlinear equations at the crown level, applicable to all selected species in the evergreen and deciduous groupings, yielded the most accurate biomass estimates. The results indicated that the crown-level spectral responses provided adequate information for delivering spatially explicit biomass estimation in highly fragmented urban landscapes with minimum field effort. Future research should focus on developing efficient methods for crown delineation by taking advantage of the recent progress in high-resolution multispectral and LiDAR remote sensing.

Funding: This research was funded by the Intramural Research Grants from the California State University, Fullerton.

Acknowledgments: The author wishes to thank John Carroll for advice. Special thanks go to Michael Shensky for coordinating field campaigns. A number of graduate and undergraduate students helped with tree data collection, including Kelly Fair, Scott Fretwell, Adam Aaron, Andrew Shensky, Jenna Oshita, Veronica Roach, and Zaki Molvi. The author thanks their valuable assistance with field measurement. The author also greatly appreciates the constructive suggestions of the three anonymous reviewers.

Conflicts of Interest: The author declares no conflict of interest.

References

1. Nowak, D.J.; Greenfield, E.J. US urban forest statistics, values, and projections. *J. For.* **2018**, *116*, 164–177. [CrossRef]
2. United Nations Population Division. *World Urbanization Prospects*; United Nations Department of Economic and Social Affairs: New York, NY, USA, 2018.
3. Bolund, P.; Hunhammar, S. Ecosystem services in urban areas. *Ecol. Econ.* **1999**, *29*, 293–301. [CrossRef]
4. Wilson, B.; Chakraborty, A. The environmental impacts of sprawl: Emergent themes from the past decade of planning research. *Sustainability* **2013**, *5*, 3302–3327. [CrossRef]
5. Andersson, E. Urban landscapes and sustainable cities. *Ecol. Soc.* **2006**, *11*, 34:1–34:17. [CrossRef]

6. Cohen, M. A systematic review of urban sustainability assessment literature. *Sustainability* **2017**, *9*, 2048. [CrossRef]
7. Habitat III. New Urban Agenda 2016. Available online: https://habitat3.org/the-new-urban-agenda/ (accessed on 2 June 2019).
8. Gómez, F.; Jabaloyes, J.; Montero, L.; De Vicente, V.; Valcuende, M. Green areas, the most significant indicator of the sustainability of cities: Research on their utility for urban planning. *J. Urban Plan. Dev.* **2011**, *137*, 311–328. [CrossRef]
9. McPherson, E.G.; Simpson, J.R.; Xiao, Q.; Wu, C. *Los Angeles 1-Million Tree Canopy Cover Assessment (General Technical Report PSW-GTR-207)*; USDA Forest Service, Pacific Southwest Research Station: Albany, CA, USA, 2008.
10. Grove, J.M.; O'Neil-Dunne, J.; Pelletier, K.; Nowak, D.; Walton, J. *A Report on New York City's Present and Possible Urban Tree Canopy*; USDA Forest Service, Northern Research Station: Newtown Square, PA, USA, 2006.
11. Roy, S.; Byrne, J.; Pickering, C. A systematic quantitative review of urban tree benefits, costs, and assessment methods across cities in different climatic zones. *Urban For. Urban Green.* **2012**, *11*, 351–363. [CrossRef]
12. Tzoulas, K.; Korpela, K.; Venn, S.; Yli-Pelkonen, V.; Kaźmiercak, A.; Niemela, J.; James, P. Promoting ecosystem and human health in urban areas using greenspace infrastructure: A literature review. *Landsc. Urban Plan.* **2007**, *81*, 167–178. [CrossRef]
13. Salmond, J.J.A.; Tadaki, M.; Vardoulakis, S.; Arbuthnott, K.; Coutts, A.; Demuzere, M.; Dirks, K.N.; Heaviside, C.; Lim, S.; Macintyre, H.; et al. Health and climate related ecosystem services provided by street trees in the urban environment. *Environ. Health* **2016**, *15*, 36:1–36:17. [CrossRef] [PubMed]
14. Gómez-Baggethun, E.; Gren, A.; Barton, D.N.; Langemeyer, J.; McPhearson, T.; O'Farrell, P.; Andersson, E.; Hamstead, Z.; Kremer, P. Urban ecosystem services. In *Urbanization, Biodiversity and Ecosystem Services: Challenges and Opportunities: A Global Assessment*; Elmqvist, T., Fragkias, M., Goodness, J., Güneralp, B., Marcotullio, P.J., McDonald, R.I., Parnell, S., Schewenius, M., Sendstad, M., Seto, K.C., et al., Eds.; Springer: New York, NY, USA, 2013; pp. 175–251. ISBN 978-94-007-7087-4.
15. Ordóñez, C.; Duinker, P.N. Interpreting sustainability for urban forests. *Sustainability* **2010**, *2*, 1510–1522. [CrossRef]
16. Millennium Ecosystem Assessment. *Ecosystems and Human Well-being: Synthesis*; Island Press: Washington, DC, USA, 2005; ISBN 1-59726-040-1.
17. MacFarlane, D.W. Potential availability of urban wood biomass in Michigan: Implications for energy production, carbon sequestration and sustainable forest management in the USA. *Biomass Bioenergy* **2009**, *33*, 628–634. [CrossRef]
18. Nowak, D.J.; Greenfield, E.J.; Hoehn, R.E.; Lapoint, E. Carbon storage and sequestration by trees in urban and community areas of the United States. *Environ. Pollut.* **2013**, *178*, 229–236. [CrossRef] [PubMed]
19. Abdollahi, K.K.; Ning, Z.H.; Appeaning, A. *Global Climate Change and the Urban Forest*; GCRCC and Franklin Press: Baton Rouge, LA, USA, 2000; ISBN 978-193-012-962-7.
20. Gill, S.E.; Handley, J.F.; Ennos, A.R.; Pauleit, S. Adapting cities for climate change: The role of the green infrastructure. *Built Environ.* **2007**, *33*, 115–133. [CrossRef]
21. Escobedo, F.J.; Nowak, D.J. Spatial heterogeneity and air pollution removal by an urban forest. *Landsc. Urban Plan.* **2009**, *90*, 102–110. [CrossRef]
22. Nowak, D.J.; Hirabayashi, S.; Bodine, A.; Greenfield, E. Tree and forest effects on air quality and human health in the United States. *Environ. Pollut.* **2014**, *193*, 119–129. [CrossRef] [PubMed]
23. Pauleit, S.; Duhme, F. Assessing the environmental performance of landcover types for urban planning. *Landsc. Urban Plan.* **2000**, *52*, 1–20. [CrossRef]
24. Chiesura, A. The role of urban parks for the sustainable city. *Landsc. Urban Plan.* **2004**, *68*, 129–138. [CrossRef]
25. Chan, K.M.A.; Satterfield, T.; Goldstein, J. Rethinking ecosystem services to better address and navigate cultural values. *Ecol. Econ.* **2012**, *74*, 8–18. [CrossRef]
26. Alvey, A.A. Promoting and preserving biodiversity in the urban forest. *Urban For. Urban Green.* **2006**, *5*, 195–201. [CrossRef]
27. Engemann, K.; Pedersen, C.B.; Arge, L.; Tsirogiannis, C.; Mortensen, P.B.; Svenning, J.-C. Residential green space in childhood is associated with lower risk of psychiatric disorders from adolescence into adulthood. *Proc. Natl. Acad. Sci. USA* **2019**, *116*, 5188–5193. [CrossRef]

28. Luederitz, C.; Brink, E.; Gralla, F.; Hermelingmeier, V.; Meyer, M.; Niven, L.; Panzer, L.; Partelow, S.; Rau, A.-L.; Sasaki, R.; et al. A review of urban ecosystem services: Six key challenges for future research. *Ecosyst. Serv.* **2015**, *14*, 98–112. [CrossRef]
29. Buccolieri, R.; Santiago, J.; Rivas, E.; Sanchez, B. Review on urban tree modelling in CFD simulations: Aerodynamic, deposition and thermal effects. *Urban For. Urban Green.* **2018**, *31*, 212–220. [CrossRef]
30. Janhäll, S. Review on urban vegetation and particle air pollution—Deposition and dispersion. *Atmos. Environ.* **2015**, *105*, 130–137. [CrossRef]
31. Xiao, Q.; McPherson, E.G. Surface water storage capacity of twenty tree species in Davis, California. *J. Environ. Qual.* **2016**, *45*, 188–198. [CrossRef]
32. Mitraka, Z.; Diamantakis, E.; Chrysoulakis, N.; Castro, E.A.; Jose, R.S.; Gonzalez, A.; Blecic, I. Incorporating bio-physical sciences into a decision support tool for sustainable urban planning. *Sustainability* **2014**, *6*, 7982–8006. [CrossRef]
33. Chrysoulakis, N.; Lopes, M.; García, R.; Grimmond, C.; Jones, M.; Magliulo, V.; Klostermann, J.; Synnefa, A.; Mitraka, Z.; Castro, E.; et al. Sustainable urban metabolism as a link between bio-physical sciences and urban planning: The BRIDGE project. *Landsc. Urban Plan.* **2013**, *112*, 100–117. [CrossRef]
34. MacKenzie, R.; Pugh, T.; Rogers, C. Sustainable cities: Seeing past the trees. *Nature* **2010**, *468*, 765. [CrossRef]
35. Pataki, D.E. City trees: Urban greening needs better data. *Nature* **2013**, *502*, 624. [CrossRef]
36. USDA Forest Service. *Forest Inventory and Analysis, National Urban FIA Plot Field Guide: Field Data Collection Procedures for Urban FIA Plots, version 7.2.1*; USDA Forest Service: Washington, DC, USA, 2018.
37. Brown, S.; Gillespie, A.; Lugo, A.E. Biomass estimation methods for tropical forests with applications to forest inventory data. *For. Sci.* **1989**, *35*, 881–902. [CrossRef]
38. Jenkins, J.C.; Chojnacky, D.C.; Heath, L.S.; Birdsey, R.A. *Comprehensive Database of Diameter-based Biomass Regressions for North American Tree Species (General Technical Report NE-319)*; USDA Forest Service, Northeastern Research Station: Newtown Square, PA, USA, 2004.
39. Chojnacky, D.C.; Heath, L.S.; Jenkins, J.C. Updated generalized biomass equations for North American tree species. *Forestry* **2014**, *87*, 129–151. [CrossRef]
40. Jenkins, J.C.; Chojnacky, D.C.; Heath, L.S.; Birdsey, R.A. National scale biomass estimators for United States tree species. *For. Sci.* **2003**, *49*, 12–35. [CrossRef]
41. Ter-Mikaelian, M.T.; Korzukhin, M.D. Biomass equations for sixty-five North American tree species. *For. Ecol. Manag.* **1997**, *97*, 1–24. [CrossRef]
42. Pillsbury, N.H.; Reimer, J.L.; Thompson, R.P. *Tree Volume Equations for Fifteen Urban Species in California (Technical Report No. 7)*; Urban Forest Ecosystems Institute, California Polytechnic State University: San Luis Obsipo, CA, USA, 1998.
43. McHale, M.R.; Burke, I.C.; Lefsky, M.A.; Peper, P.J.; McPherson, E.G. Urban forest biomass estimates: Is it important to use allometric relationships developed specifically for urban trees? *Urban Ecosyst.* **2009**, *12*, 95–113. [CrossRef]
44. Nowak, D.J.; Crane, D.E. The urban forest effects (UFORE) model: Quantifying urban forest structure and functions. In *Integrated Tools for Natural Resources Inventories in the 21st Century (General Technical Report NC-212)*; Hansen, M., Burk, T., Eds.; USDA Forest Service, North Central Forest Experiment Station: St. Paul, MN, USA, 2000; pp. 714–720.
45. Nowak, D.J.; Crane, D.E.; Stevens, J.C.; Ibarra, M. *Brooklyn's Urban Forest (General Technical Report NE-290)*; USDA Forest Service, Northeastern Research Station: Newtown Square, PA, USA, 2002.
46. Jo, H.-K.; McPherson, E.G. Carbon storage and flux in urban residential greenspace. *J. Environ. Manag.* **1995**, *45*, 109–133. [CrossRef]
47. Nowak, D.J.; Crane, D.E.; Stevens, J.C.; Hoehn, R.E.; Walton, J.T.; Bond, J. A ground-based method of assessing urban forest structure and ecosystem services. *Arboric. Urban For.* **2008**, *34*, 347–358.
48. McPherson, E.G.; Simpson, J.R.; Peper, P.J.; Maco, S.E.; Xiao, Q. Municipal forest benefits and costs in five US cities. *J. For.* **2005**, *103*, 411–416. [CrossRef]
49. Aguaron, E.; Mcpherson, E.G. Comparison of methods for estimating carbon dioxide storage in Sacramento's urban forest. In *Carbon Sequestration in Urban Ecosystems*; Lal, R., Augustin, B., Eds.; Springer: New York, NY, USA, 2012; pp. 43–71. ISBN 978-94-007-2365-8.
50. Peper, P.J.; McPherson, E.G. Comparison of four foliar and woody biomass estimation methods applied to open-grown deciduous trees. *J. Arboric.* **1998**, *24*, 191–200.

51. Nowak, D.J. Atmospheric carbon dioxide reduction by Chicago's urban forest. In *Chicago's Urban Forest Ecosystem: Results of the Chicago Urban Forest Climate Project (General Technical Report NE-186)*; McPherson, E.G., Nowak, D.J., Rowntree, R.A., Eds.; USDA Forest Service, Northeastern Forest Experiment Station: Radnor, PA, USA, 1994; pp. 83–94.
52. Nowak, D.J.; Crane, D.E. Carbon storage and sequestration by urban trees in the USA. *Environ. Pollut.* **2002**, *116*, 381–389. [CrossRef]
53. Pastor, J.; Aber, J.D.; Melillo, J.M. Biomass prediction using generalized allometric regressions for some northeast tree species. *For. Ecol. Manag.* **1984**, *7*, 265–274. [CrossRef]
54. Tigges, J.; Churkina, G.; Lakes, T. Modeling above-ground carbon storage: A remote sensing approach to derive individual tree species information in urban settings. *Urban Ecosyst.* **2017**, *20*, 97–111. [CrossRef]
55. McPherson, E.G.; van Doorn, N.S.; Peper, P.J. *Urban Tree Database and Allometric Equations (General Technical Report PSW-GTR-253)*; USDA Forest Service, Pacific Southwest Research Station: Albany, CA, USA, 2016.
56. Kunwar, K.S.; Chen, G.; McCarter, J.B.; Meentemeyer, R.K. Effects of LiDAR point density and landscape context on estimates of urban forest biomass. *ISPRS J. Photogramm. Remote Sens.* **2015**, *101*, 310–322. [CrossRef]
57. McPherson, E.G.; Xiao, Q.; Aguaron, E. A new approach to quantify and map carbon stored, sequestered and emissions avoided by urban forests. *Landsc. Urban Plan.* **2013**, *120*, 70–84. [CrossRef]
58. Raciti, S.M.; Hutyra, L.R.; Newell, J.D. Mapping carbon storage in urban trees with multi-source remote sensing data: Relationships between biomass, land use, and demographics in Boston neighborhoods. *Sci. Total Environ.* **2014**, *500–501*, 72–83. [CrossRef] [PubMed]
59. Myeong, S.; Nowak, D.J.; Duggin, M.J. A temporal analysis of urban forest carbon storage using remote sensing. *Remote Sens. Environ.* **2006**, *101*, 277–282. [CrossRef]
60. Wilkes, P.; Disney, M.I.; Vicari, M.B.; Calders, K.; Burt, A. Estimating urban above ground biomass with multi-scale LiDAR. *Carbon Balance Manag.* **2018**, *13*, 10:1–10:20. [CrossRef] [PubMed]
61. Alonzo, M.; McFadden, J.P.; Nowak, D.J.; Roberts, D.A. Mapping urban forest structure and function using hyperspectral imagery and LiDAR data. *Urban For. Urban Green.* **2016**, *17*, 135–147. [CrossRef]
62. Shrestha, R.; Wynne, R.H. Estimating biophysical parameters of individual trees in an urban environment using small footprint discrete-return imaging LiDAR. *Remote Sens.* **2012**, *4*, 484–508. [CrossRef]
63. Lee, J.-H.; Ko, Y.; McPherson, E.G. The feasibility of remotely sensed data to estimate urban tree dimensions and biomass. *Urban For. Urban Green.* **2016**, *16*, 208–220. [CrossRef]
64. Chen, X.; Ye, C.; Li, J.; Chapman, M.A. Quantifying the carbon storage in urban trees using multispectral ALS data. *IEEE J. Sel. Top. Appl. Earth Obs. Remote Sens.* **2018**, *11*, 3358–3365. [CrossRef]
65. Fassnacht, F.E.; Latifi, H.; Stereńczak, K.; Modzelewska, A.; Lefsky, M.; Waser, L.T.; Straub, C.; Ghosh, A. Review of studies on tree species classification from remotely sensed data. *Remote Sens. Environ.* **2016**, *186*, 64–87. [CrossRef]
66. Alonzo, M.; Bookhagen, B.; Roberts, D.A. Urban tree species mapping using hyperspectral and LiDAR data fusion. *Remote Sens. Environ.* **2014**, *148*, 70–83. [CrossRef]
67. Voss, M.; Sugumaran, R. Seasonal effect on tree species classification in an urban environment using hyperspectral data, LiDAR, and an object-oriented approach. *Sensors* **2008**, *8*, 3020–3036. [CrossRef] [PubMed]
68. Zhang, C.; Qiu, F. Mapping individual tree species in an urban forest using airborne LiDAR data and hyperspectral imagery. *Photogramm. Eng. Remote Sens.* **2012**, *78*, 1079–1087. [CrossRef]
69. Liu, L.; Coops, N.C.; Aven, N.W.; Pang, Y. Mapping urban tree species using integrated airborne hyperspectral and LiDAR remote sensing data. *Remote Sens. Environ.* **2017**, *200*, 170–182. [CrossRef]
70. Zhang, Z.; Kazakova, A.; Moskal, M.L.; Styers, M.D. Object-based tree species classification in urban ecosystems using LiDAR and hyperspectral data. *Forests* **2016**, *7*, 122. [CrossRef]
71. Grimm, N.B.; Faeth, S.H.; Golubiewski, N.E.; Redman, C.L.; Wu, J.; Bai, X.; Briggs, J.M. Global change and the ecology of cities. *Science* **2008**, *319*, 756–760. [CrossRef]
72. Myint, S.W.; Gober, P.; Brazel, A.J.; Grossman-Clarke, S. Per-pixel vs. object-based classification of urban land cover extraction using high spatial resolution imagery. *Remote Sens. Environ.* **2011**, *115*, 1145–1161. [CrossRef]
73. Wu, J.; Bauer, M.E. Estimating net primary production of turfgrass in an urban-suburban landscape with quickbird imagery. *Remote Sens.* **2012**, *4*, 849–866. [CrossRef]

74. Wu, J.; Bauer, M.E. Evaluating the effects of shadow detection on Quickbird image classification and spectroradiometric restoration. *Remote Sens.* **2013**, *5*, 4450–4469. [CrossRef]
75. Richardson, J.; Moskal, L. Uncertainty in urban forest canopy assessment: Lessons from Seattle, WA, USA. *Urban For. Urban Green.* **2014**, *13*, 152–157. [CrossRef]
76. Chen, G.; Ozelkan, E.; Singh, K.K.; Zhou, J.; Brown, M.R.; Meentemeyer, R.K. Uncertainties in mapping forest carbon in urban ecosystems. *J. Environ. Manag.* **2017**, *187*, 229–238. [CrossRef] [PubMed]
77. Myeong, S.; Nowak, D.J.; Hopkins, P.F.; Brock, R.H. Urban cover mapping using digital high-spatial resolution aerial imagery. *Urban Ecosyst.* **2001**, *5*, 243–256. [CrossRef]
78. Pu, R.; Landry, S. A comparative analysis of high spatial resolution IKONOS and WorldView-2 imagery for mapping urban tree species. *Remote Sens. Environ.* **2012**, *124*, 516–533. [CrossRef]
79. Li, D.; Ke, Y.; Gong, H.; Li, X. Object-based urban tree species classification using bi-temporal WorldView-2 and WorldView-3 images. *Remote Sens.* **2015**, *7*, 16917–16937. [CrossRef]
80. Shojanoori, R.; Shafri, H.Z.M. Review on the Use of Remote Sensing for Urban Forest Monitoring. *Arboric. Urban For.* **2016**, *42*, 400–417.
81. Wulder, M.; Niemann, K.O.; Goodenough, D. Local maximum filtering for the extraction of tree locations and basal area from high spatial resolution imagery. *Remote Sens. Environ.* **2000**, *73*, 103–114. [CrossRef]
82. Xiao, Q.; Ustin, S.L.; McPherson, E.G. Using AVIRIS data and multiple-masking techniques to map urban forest species. *Int. J. Remote Sens.* **2004**, *25*, 5637–5654. [CrossRef]
83. Wu, J.; Wang, D.; Bauer, M.E. Image-based atmospheric correction of QuickBird imagery of Minnesota cropland. *Remote Sens. Environ.* **2005**, *99*, 315–325. [CrossRef]
84. Updike, T.; Comp, C. Radiometric use of WorldView-2 imagery. In *DigitalGlobe Technical Note*; DigitalGlobe, Inc.: Westminster, CO, USA, 2010.
85. Shensky, M.G., Jr. Designing Field Data Collection Methods for Developing a University Enterprise GIS Database: An Assessment of the California State University, Fullerton Tree Inventory. Master's Thesis, California State University, Fullerton, CA, USA, 2013.
86. Wilkinson, D.M. Modelling tree crowns as geometric solids. *Arboric. J.* **1995**, *19*, 387–393. [CrossRef]
87. Beyer, H.L. Geospatial Modelling Environment, version 0.7.4.0. Available online: http://www.spatialecology.com/gme (accessed on 11 October 2018).
88. ESRI. *ArcGIS Desktop, Release 10.3.1*; Environmental Systems Research Institute: Redlands, CA, USA, 2014.
89. Climate Action Reserve. *Urban Forest Project Protocol, version 1.1*; Climate Action Reserve: Los Angeles, CA, USA, 2010.
90. Markwardt, L.J.; Wilson, T.R. *Strength and Related Properties of Woods Grown in the United States (Technical Bulletin No. 479)*; USDA Forest Service, Forest Products Laboratory: Madison, WI, USA, 1935.
91. Cairns, M.A.; Brown, S.; Helmer, E.H.; Baumgardnerl, G.A. Root biomass allocation in the world's upland forests. *Oecologia* **1997**, *111*, 1–11. [CrossRef]
92. Husch, B.; Beers, T.W.; Kershaw, J.A., Jr. *Forest Mensuration*, 4th ed.; Wiley: New York, NY, USA, 2002; ISBN 978-0-471-01850-6.
93. Rouse, J.W.; Haas, R.H., Jr.; Schell, J.A.; Deering, D.W. Monitoring vegetation systems in the Great Plains with ERTS. In *3rd ERTS-1 Symposium*; NASA SP-351; NASA: Washington, DC, USA, 1974; Volume 1, pp. 309–317.
94. Brandtberg, T.; Walter, F. Automated delineation of individual tree crowns in high spatial resolution aerial images by multiple-scale analysis. *Mach. Vis. Appl.* **1998**, *11*, 64–73. [CrossRef]
95. Parresol, B.R. Assessing tree and stand biomass: A review with examples and critical comparisons. *For. Sci.* **1999**, *45*, 573–593. [CrossRef]
96. Baskerville, G.L. Use of logarithmic regression in the estimation of plant biomass. *Can. J. For. Res.* **1972**, *2*, 49–53. [CrossRef]
97. IBM Corporation. *IBM SPSS Statistics for Windows*; Release 25.0; IBM Corporation: Armonk, NY, USA, 2017.
98. Crow, T.R.; Schlaegel, B.E. A guide to using regression equations for estimating tree biomass. *North. J. Appl. For.* **1988**, *5*, 15–22. [CrossRef]
99. Rao, P.; Hutyra, L.R.; Raciti, S.M.; Finzi, A.C. Field and remotely sensed measures of soil and vegetation carbon and nitrogen across an urbanization gradient in the Boston metropolitan area. *Urban Ecosyst.* **2013**, *16*, 593–616. [CrossRef]
100. Beauchamp, J.J.; Olson, J.S. Corrections for bias in regression estimates after logarithmic transformation. *Ecology* **1973**, *54*, 1403–1407. [CrossRef]

101. Sprugel, D.G. Correcting for bias in long-transformed allometric equations. *Ecology* **1983**, *64*, 209–210. [CrossRef]
102. Shaw, J.D. Models for estimation and simulation of crown and canopy cover. In Proceedings of the Fifth Annual Forest Inventory and Analysis Symposium (General Technical Report WO-69), New Orleans, LA, USA, 18–20 November 2003; pp. 183–191.
103. Lang, M.; Kurvits, V. Restoration of tree crown shape for canopy cover estimation. *For. Stud.* **2007**, *46*, 23–34.
104. Johnson, A.D.; Gerhold, H.D. Carbon storage by urban tree cultivars, in roots and above-ground. *Urban For. Urban Green.* **2003**, *2*, 65–72. [CrossRef]
105. Nyakuengama, J.G.; Downes, G.M.; Ng, J. Growth and wood density responses to later-age fertilizer application in Pinus radiata. *IAWA J.* **2002**, *23*, 431–448. [CrossRef]